Computer-aided Capsule Endoscopy Images Evaluation based on Color Rotation and Texture Features: An educational tool to physicians

Vasileios S. Charisis
Electrical and Computer Engineering Dept., Aristotle University of Thessaloniki, Greece,

Christina Katsimerou
Electrical and Computer Engineering Dept., Aristotle University of Thessaloniki, Greece,

Leontios J. Hadjileontiadis
Electrical and Computer Engineering Dept., Aristotle University of Thessaloniki, Greece,

Christos N. Liatsos
401 Army General Hospital of Athens, Greece

George D. Sergiadis
Electrical and Computer Engineering Dept, Aristotle University of Thessaloniki, Greece,

Abstract

Wireless capsule endoscopy (WCE) is a revolutionary, patient-friendly imaging technique that enables non-invasive visual inspection of the patient's digestive tract and, especially, small intestine. However, reviewing the endoscopic data is time consuming and requires intense labor of highly experienced physicians. These limitations were the motive to propose a novel strategy for automatic discrimination of WCE images related to ulcer, the most common finding of digestive tract. Towards this direction, WCE data are color-rotated in order to boost the chromatic attributes of ulcer regions. Then, texture information is extracted by utilizing the local binary pattern operator that analyses the spatial structure of the images at a very local level. Experimental results demonstrated promising classification accuracy (91.1%) exhibiting high potential towards a complete computer-aided diagnosis system that will not only reduce WCE data reviewing time, but also serve as an assisting tool for the training of inexperienced physicians.

1. Introduction

The recently established Wireless Capsule Endoscopy (WCE) [1] has marked a revolution in the field of gastroenterology, beginning an era of comfortable visualization of the entire gastrointestinal (GI) tract, even the middle part of small intestine [2]. The innovative endoscopic capsule travels through the GI tract capturing and wirelessly transmitting more than 55000 frames. At the end of the examination these images, which are temporarily stored in a wearable data recorder, are downloaded to a computer and reviewed by the physician.

WCE has proven invaluable in evaluating various diseases of the small bowel [2]. One of the most common GI findings efficiently detected by WCE is ulcer. Approximately 10% of the people suffer from ulcerations. The most usual causes are Helicobacter pylori bacteria and use of nonsteroidal anti-inflammatory drugs (NSAID). Ulcer is not lethal; however serious diseases are associated with it, such as Crohn's disease and ulcerative colitis. Therefore, its early diagnosis and treatment is essential.

Despite the revolutionary benefits introduced by WCE, ample room for improvement still remains. The burdensome task of inspecting the WCE images costs 1 to 2 hours of intense labor for an expert who needs to stay focused for such a long time. Moreover, abnormalities may appear in only one or two frames and be easily missed due to oversight or inexperience. These limitations inspire researchers to develop computer assisting systems to reduce the workload of the physicians and, consequently, the cost of the examination. Moreover, computer assisted diagnosis may augment the medical education of trainee physicians and enable the practice of such a novel endoscopic technique by less experienced gastroenterologists.

Many efforts towards WCE analysis have been reported in the literature. The majority of them aim to automatically detect abnormalities. The techniques proposed for tumor and polyp detection include texture spectrum along with neural networks [3], [4],

geometric and texture features based on co-occurrence matrices [5], Gabor filters along with SUSAN edge detectors [6], wavelet-based local binary pattern analysis (LBP) [7] and rotation invariant uniform LBP [4]. Texture and color features extracted from various color spaces have contributed to ulcer recognition. In particular, ulcer has been detected by applying LBP along with color moment invariants [8], curvelet-based LBP [9], color channel histograms [10], texture unit number transform and texture spectrum [11], Log-Gabor filters combined with statistical texture characteristics [8] and color wavelet covariance [12]. Moreover, ulcer detection is achieved by processing WCE images in RGB, HSV and CIE Lab color spaces with ensemble empirical mode decomposition [13], and adaptive lacunarity analysis [14].

In this work, the aim is not only to propose a novel approach for automatic ulcer region detection, but also to examine and evaluate, for the first time to the best of our knowledge, its actual benefit to physicians of various experience backgrounds. Thus, a color rotation – texture extraction scheme is introduced for WCE image analysis and computerized diagnosis. WCE data are color-rotated in order to optimize the projection of ulcer characteristics on the chromatic planes. Then, texture features are extracted through rotation invariant uniform local binary pattern operator that analyses the distribution of pattern primitives inherent in any surface. The texture analysis output is classified into healthy and ulcerous with the aid of Support Vector Machines.

2. Methodology

2.1. Color rotation

Each image pixel consists of a three-dimensional vector that determines its color. One of the most efficient color spaces for WCE-based ulcer detection is the hardware-based Red-Green-Blue (RGB) [13]. Consider a pixel *x(r,g,b)* in RGB space where *r, g, b* are its red, green, blue color components (coordinates). A rotated version of *x* is a pixel *x'* in a new position *(r',g',b')* in RGB space and is defined as: $x'=R_{rgb}\cdot x$ where R_{rgb} is the color rotation matrix. R_{rgb} is defined as $R_{rgb}=R_r\cdot R_g\cdot R_b$ where

$$R_r=\begin{bmatrix}1 & 0 & 0\\ 0 & \cos(a) & \sin(a)\\ 0 & -\sin(a) & \cos(a)\end{bmatrix}, \quad (1)$$

$$R_g=\begin{bmatrix}\cos(b) & 0 & -\sin(b)\\ 0 & 1 & 0\\ \sin(b) & 0 & \cos(b)\end{bmatrix}, \quad (2)$$

$$R_b=\begin{bmatrix}\cos(c) & \sin(c) & 0\\ -\sin(c) & \cos(c) & 0\\ 0 & 0 & 1\end{bmatrix} \quad (3)$$

and *a, b, c* are the rotation angles around R, G, B axis, respectively. Rotating the pixels of a given image I_{init} results in a new, non-normalized, color rotated image I_{rot}. The final normalized image is calculated by:

$$I_{norm}=(I_{rot}-I_{rot}^{\max})/(I_{rot}^{\max}-I_{rot}^{\min})*255, \quad (4)$$

where I_{rot}^{max} and I_{rot}^{min} are the highest and lowest pixel values of I_{rot}.

Color is a major feature of images in automatic content extraction and characterization procedure. The concept of color rotation is based on the idea of remapping chromatic content towards specific color planes. The purpose is to meliorate and optimize the projection of the content-of-interest on more informative color planes and promote the extraction of intrinsic characteristics that will facilitate the discrimination process. Color rotation has the advantage of preserving the pixel relationships and the overall character of the image by maintaining the relative positions of pixel vectors since mapping from a basis [1 0 0;0 1 0;0 0 1] to another Euclidean Space's basis [R_r, R_g, R_b] takes place.

2.2. Local binary pattern

The well known local binary pattern (LBP) texture operator, proposed by Ojala et al. [15], is defined as a grayscale invariant texture measure, derived from a general definition of texture in a local neighborhood. This technique is based on a two level version of texture spectrum method, and describes the spatial structures of local image texture. First, each pixel in an image is labeled by an 8-bit binary code that is produced by thresholding the difference between the central pixel and its 8 neighbors (3x3 neighborhood). Then, pixel values in the thresholded neighborhood are multiplied by binomial weights given to corresponding pixels. The values of the products are summed up to obtain the LBP number of this neighborhood. Finally, a histogram is created to collect up the occurrences of different LBP patterns (up to 2^8).

This basic version of LBP is extended to a multiresolution analysis tool that includes not only the 3x3 neighborhood but also any circularly symmetric neighbor set of P members on a circle of radius R, as illustrated in Fig. 1, where P and R denote the quantization of the angular space and spatial resolution. The $LBP_{P,R}$ number is defined as:

$$LBP_{P,R}=\sum_{p=0}^{P-1}s(g_p-g_c)2^p \quad (5)$$

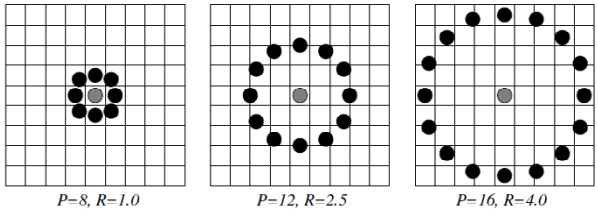

Figure 1. Circularly symmetric neighbors.

where s(x) is the sign function and g_c, g_p the values of central and neighboring pixels. In order to remove effects of rotation and base neighbor (p=0) selection a rotation invariant LBP (LBP^{ri}) is introduced [16] as:

$$LBP^{ri} = \min(ROR(LBP_{P,R}, i)), i = 0...P-1 \quad (6)$$

where ROR(x,i) operates a circular bit-wise right-shift on a P-bit LBP number x i times. All rotated versions of the same patterns are grouped into much less rotation invariant structures that correspond to certain micro-features of the images. Moreover, the 256 bins of the initial LBP histogram are reduced to 36 (when P=8).

It is observed that some local binary patterns are fundamental as they take up the vast majority of the image local binary patterns. These fundamental patterns are called "uniform" since they exhibit uniform circular structure that contains very few spatial transitions (bitwise 1/0 changes). In this context, a new uniform LBP^{ri} (LBP^{riu2}) is proposed [16] as:

$$LBP^{riu2} = \begin{cases} \sum_{p=0}^{P-1} s(g_p - g_c), U(LBP_{P,R}) \le 2 \\ P+1, \quad otherwise \end{cases} \quad (7)$$

where $U(LBP_{P,R})$ is the number of 1/0 changes. By definition, P+1 uniform binary patterns can occur in a circularly symmetric neighbor set of P pixels. Eq. (7) assigns a unique label to each of them according to the number of "1" bits in the pattern while the nonuniform patterns are grouped under the miscellaneous P+1.

2.3. Proposed approach

The aim of this work is the color-texture-based detection of ulcer tissue from WCE data. The color-texture concept was motivated by physicians' clinical practice, where the color and texture properties of WCE data are utilized for reaching a diagnosis. A flow chart of the proposed approach is shown in Fig. 2.

The first step of the proposed approach is color rotation (CR). The gravity of color information in eliciting efficient diagnostic content is depicted in the researchers' efforts as reported in the literature. GI diseases are characterized by various colors. For example, active bleeding is designated by deep red hues on the light yellow-red-pink healthy mucous

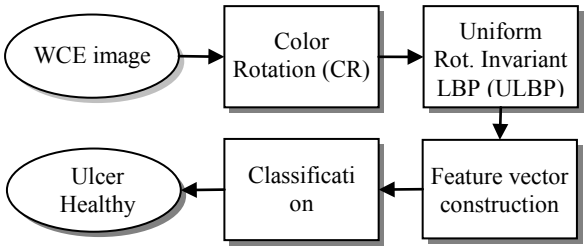

Figure 2. The proposed CR-ULBP scheme.

membranes, while ulcerations exhibit yellow-greenish appearance. Moreover, previous studies have shown that the majority of ulcer information lie on green channel [13], [14]. These observations were the rationale to apply CR to augment the content of the green plane and facilitate texture extraction.

Color information of WCE images may be misleading owing to uneven lighting conditions inside GI tract (overexposed spots when the capsule is close to tract walls), peptic content (gastric fluids are similar in color to ulcers) and the close relationship of color to brightness. From this perspective, tissue pattern extraction is mandatory. Uniform rotation invariant LBP (ULBP) is employed to elicit efficient multiresolution and multidirectional texture structures. Healthy intestinal-tissue regions, in general, and ulcer regions, more specifically, exhibit wide diversity in size, shape and texture. Consequently, a pattern analysis tool free from directional limitations and capable to capture structural differences throughout multiple scales is required. ULBP operator is applied on every single color channel separately.

The final texture feature that constitutes the feature vector (FV) in texture analysis is the histogram of the ULBP operator output (i.e. pattern labels) accumulated over the entire image. The reason why the histogram of uniform patterns provides better discrimination in comparison to the histogram of all individual patterns comes down to differences in their statistical properties [16]. The relative proportion of nonuniform patterns of all patterns accumulated into a histogram is so small that their probabilities cannot be estimated reliably. The number of histogram bins, and consequently FV dimension, is P+2.

The last step of the CR-ULBP ulcer detection scheme is tissue classification procedure into healthy and ulcerous. Support Vector Machine (SVM) with radial basis function is adopted as it has been proven to exhibit the most efficient ulcer tissue detection [13].

3. Experimental issues and dataset

Towards a thorough analysis of the proposed texture analysis methodology, ULBP operator is applied for

various (P,R) combinations so as to identify the most efficient spatial resolution and distance. Moreover, in order to evidence the importance of CR step two FV scenarios are examined. FV contains ULBP histogram that is calculated either on the original WCE images, omitting CR stage or on the color rotated images as proposed. The classification performance is measured with the aid of accuracy (acc.), sensitivity (sens.) and specificity (spec.) indexes. Ten-fold cross validation is adopted for the training/testing of the classifier.

WCE images used in this study for the development and assessment of the CR-ULBP approach were drawn from six patients with ulcerous diseases, such as unexplained ulceration, ulceration from NSAID and Crohn's diseases, who have undertaken a WCE examination. The dataset collected consists of 100 ulcer and 100 normal images. Two experts reviewed the endoscopic video and manually isolated regions of interest (ROI), as the ones shown in Fig. 3, according to their expertise and upon mutual agreement. Moreover, the ulcer ROIs were equally divided into two classes: easy (distinct ulcers of high severity, Fig. 2a) and hard (hard to detect, low severity ulcers, Fig. 2b). It must be noted that ulcer images were obtained from 100 different events to achieve the lowest possible similarity. Furthermore, normal images depict both simple and confusing healthy tissue (folds, villus, bubbles etc.) in order to hamper the detection process.

4. Results and discussion

4.1. CR-ULBP performance evaluation

The performance of the proposed CR-ULBP scheme is evaluated through the experimental results derived from the application of the introduced approach to our dataset. To this end, results from the various classification scenarios applied not only on both ulcer cases (easy, hard), but also on their concatenation (total), are presented in this section.

Figure 4 illustrates the graphical representation of LBP and ULBP analysis for one normal and one ulcer image for various combinations of neighbors (P) and distances (R). It should be noted that the rotation invariant uniform patterns are able to describe efficiently the different types of tissue regardless of the less number of binary patterns used. The images of the ULBP cases are darker due to the small number of binary patterns, especially for the uri2 R=1, P=8 case that employs only 10 patterns. Considering the ulcer image, it is readily apparent that the more neighbors engaged the better the texture representation. Additionally, when non rotation invariant LBP is

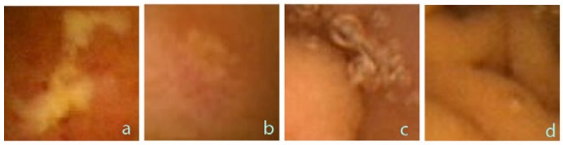

Figure 3. Example of ulcerous (a,b) and normal (c,d) regions of interest.

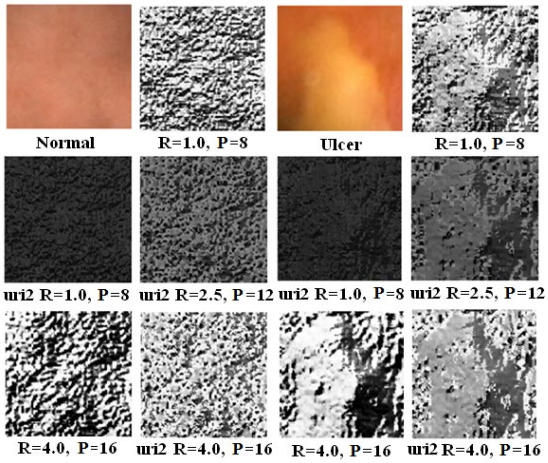

Figure 4. LBP and ULBP (uri2) representations for various R-P combinations

applied (R=4, P=16 case) the direction selectivity is blatant (left to right) creating quite dark and bright spots that may affect adversely the further analysis.

Table 1 presents the classification performance of the first classification scenario where the color rotation scheme is omitted for the three ulcer cases (easy, hard, total) . Various (R,P) combinations were examined but only the most representative are presented. FV contains the features extracted from a single color channel, i.e. R, G or B while the concatenation of these features led to inferior performance owing to the "curse of dimensionality", supposedly. Considering the (R,P) combinations it is clear that the higher the number of neighbors and their distance the better the performance. The best pair is (4,16) that delivers 88.3% acc., 91.6% sens. and 85.0% spec.. This observation coincides with the results in Fig. 4. The severity of ulcer cases plays an important role in the performance of the proposed scheme. As might be expected, ulcer detection is much more successful when ulcerations are clear rather than obscure (7.1%-G, 14.1%-B, 14.7-R higher acc. than hard case for (4,16)). As far as the color plane is concerned G proves to be the most efficient achieving the highest results for almost all scenarios. This might be explained by the fact that the reflected green light is closely related to blood volume and intestine walls are crammed with blood vessels. Case (1,8) case is an exception where channel B outperforms G, indicating that only small scale structure patterns lie on blue color

Table 1. Classification accuracy (%) for ULBP-based features without color rotation.

(R,P)*	Classification Scenario								
	R			G			B		
	Easy	Hard	Total	Easy	Hard	Total	Easy	Hard	Total
(1,8)	77.5	62.2	73.7	80.7	68.2	76.4	87.8	72.1	82.0
(2,8)	79.1	64.5	76.9	87.4	70.1	84.3	87.9	72.4	82.1
(2.5,12)	78.9	68.8	77.0	87.9	71.7	85.4	87.1	71.8	79.6
(4,16)	83.6	76.5	81.7	91.6	76.9	88.3	89.6	75.5	82.9

* R = radius of neighborhood, P = # of neighbors

that require narrower spatial resolution analysis to be detected. The variation of hard case results along R, G and B planes is subtle, designating that texture features of evolved ulcerations mainly populate G plane.

To continue, Fig. 5 illustrates the initial and color rotated versions of an ambiguous normal and a hard ulcer image as well as the green channel of the rotated images. The ulcer region is hardly recognizable in the original image while it is quite discernible after the color shifting. On the contrary, the confusing light red region in the original normal image, caused by the nonuniform illumination conditions, almost disappears. By observing G channel it can be argued that ulcer region is properly depicted whereas the ambiguity of the normal region is even smoother. It must be highlighted, though, that color rotation does not always guarantee the amelioration of the images. The angle of rotation around each color axis plays a major role to the final outcome.

The above remark is acutely depicted in Table 2 that presents the classification results when color rotation takes place. G plane and (4,16) (R,P) pair were selected since they provided with the highest rates during the previous analysis. A huge amount of rotation angles where tested but only the most exemplary are shown. The highest rates for each case are notated in boldface. By observing the classification accuracy for the various rotation angles it becomes apparent that only a few combinations manage to efficiently remap WCE chromatic data and facilitate the elicitation of ULBP-based texture features. The majority of rotation attempts led to a similar or deteriorated behavior. Typical examples for the total case are (90,0,0), (0,0,180), (0,90,180) and (180,180,0) angles that degrade the performance by 2.2% to 4.8% in terms of accuracy. On the other hand, (0,90,0) rotation delivers the highest accuracy (91.1%) and specificity (88.2%) while (0,270,0) delivers the highest sensitivity (94.9%). These angles are also the most efficient for the easy case. From an overall inspection of Table 2 we can conclude that rotation around G axis solely is the most

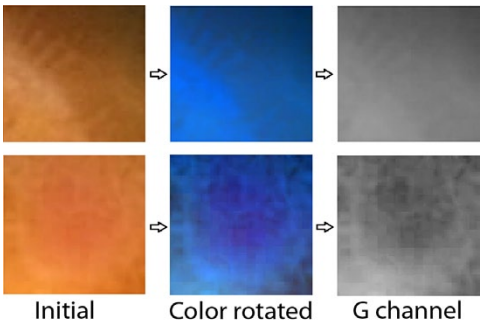

Figure 5. Color rotation (160°, 160°, 160°) of a normal (upper) and an ulcer (lower) case.

Table 2. Classification accuracy (%) for the CR-ULBP scheme for R=4, P=16 on G channel.

Rotation angles (a^o,b^o,c^o)	Ulcer case								
	Easy			Hard			Total		
	Acc.	Sens.	Spec.	Acc.	Sens.	Spec.	Acc.	Sens.	Spec.
(90,0,0)	88.1	90.7	86.8	74.9	62.8	79.5	83.5	85.8	81.1
(180,0,0)	91.2	94.2	89.5	79.9	65.3	85.6	88.0	90.9	85.2
(0,30,0)	92.4	95.1	90.9	80.5	75.9	83.5	89.1	93.0	85.1
(0,90,0)	**93.8**	95.9	**93.0**	82.6	76.3	**87.1**	**91.1**	94.0	**88.2**
(0,270,0)	92.6	**96.7**	91.5	83.1	80.8	85.4	90.4	**94.9**	85.8
(0,0,30)	90.8	95.5	88.2	79.0	65.6	84.3	87.2	91.6	82.9
(0,0,180)	87.2	90.8	85.1	75.1	62.3	80.4	85.8	92.1	79.6
(0,90,180)	87.0	90.5	84.9	72.0	57.6	76.1	83.5	86.4	80.5
(30,0,30)	91.3	94.8	88.7	80.0	70.7	83.8	87.2	91.0	83.4
(180,90,180)	93.0	95.6	92.3	**85.9**	**80.9**	86.9	90.1	92.7	87.5
(180,180,0)	90.6	94.8	89.6	81.1	73.8	83.5	86.1	91.2	81.0

competent for our goal. Nonetheless, the improvement for the easy and total case is quite limited; 93.8% instead of 91.6% and 91.1% instead of 88.3%, respectively. Conversely, color rotation is vital for the detection of low severity ulcerations. Accuracy rises from 76.9% to 85.9% for (180,90,180) rotation.

4.2. The educational role

In the direction of further testifying the performance of CR-ULBP approach and proving its grave importance to physicians' clinical practice and education we asked from 8 physicians of varying experience backgrounds to examine a test dataset of 20 WCE image patches and point out those that illustrate ulcerations. The dataset consists of 10 of the most ambiguous normal and 10 of the hardest ulcer images of our experimental dataset. Table 3 contains the diagnosis rates for each physician as well as the

Table 3. Diagnosis results of hard ulcer (10 cases) and normal images (10 cases) from 8 physicians (P1-8) and CR-ULBP scheme.

Class. index	Subject								
	P1	P2	P3	P4	P5	P6	P7	P8	App.
Acc.	45%	45%	45%	50%	95%	50%	50%	40%	75%
Sens.	20%	10%	10%	20%	90%	20%	20%	10%	70%
Spec.	70%	80%	80%	80%	100%	80%	80%	70%	80%

performance of the proposed ulcer detection scheme. It is remarkable that the majority of physicians can hardly recognize the ulcer regions (15.7% ± 5.3 mean sens. excluding subject P5 that achieved exceptional performance) while CR-ULBP scheme achieves 70% correct positive predictions. On the contrary, almost all normal images are correctly detected. Physicians are trained to recognize abnormalities by not focusing on small areas but considering various information cumulatively, i.e. edge, color, texture, and performing subconscious comparisons between the suspected abnormal and the adjacent normal tissue. The proposed automatic ulcer detection scheme, that is able to differentiate ulcer structures in a variety of scales, would be beneficial in indicating to physicians regions with suspected or imminent ulcerations towards more detailed inspection. In this direction, CR-ULBP may constitute a valuable tool for the training of junior physicians or gastroenterologists without experience in capsule endoscopy.

5. Conclusion

This work presents an innovative CR-ULBP scheme for WCE image analysis. Efficient color rotation is combined with novel uniform rotation invariant LBP towards effective ulcer detection. Experiments highlighted that appropriate color shifting enhances the patterns of low severity ulcers. The diagnostic performance of the proposed scheme was compared to that of 8 physicians, based on a test-set of 20 very hard ulcer and normal image patches, and exhibited fairly encouraging results. The advanced overall performance of the introduced ulcer detection scheme (91.1% accuracy) paves the way for its use in a provisional automatic diagnosis system that will be of great service for physicians' training and everyday clinical practise.

6. References

[1] G. Iddan, G. Meron, A. Glukhovsky, and P. Swain, "Wireless capsule endoscopy," *Nature*, vol. 405, no. 6785, pp. 405-417, 2000.

[2] M. Pennazio, "Diagnosis of small-bowel diseases in the era of capsule endoscopy, *Expert Rev. Med. Dev.*, vol. 2, no. 5, pp. 587–598, 2005.

[3] V. Kodogiannis, M. Boulougoura, J. Lygouras, and I. Petrounias, "A neuro-fuzzy-based system for detecting abnormal patterns in wireless-capsule endoscopic images," *Neurocomputing*, vol. 70, pp. 704-717, 2007

[4] B. Li and Max Q.-H. Meng, "Comparison of several texture features for tumor detection in CE iamges, " *J Med Syst*, vol. 36, pp. 2463-2469, 2012.

[5] S.A. Karkanis *et al.*, "Computer-aided tumor detection in endoscopic video using color wavelet features," *IEEE Trans. Inf. Tech. Biomed*., vol. 7, pp. 141-152, 2003.

[6] A. Karargyris and N. Bourbakis, "Detection of small bowel polyps and ulcers in wireless capsule endoscopy videos", *IEEE Trans on Biomed. Eng.*, vol. 58, no. 10, pp. 2777-2786, 2011.

[7] B. Li, M.Q.-H. Meng, and J.Y.W. Lau, "Computer-aided small bowel tumor detection for capsule endoscopy", *Artif. Intel. Med.*, vol. 52, pp. 11-16, 2011.

[8] D. Chen, *et al.*, "A novel strategy to label abnormalities for wireless capsule endoscopy frames sequence," in *Proc. 2011 Int. Conf. IEEE Inf. Autom.*, Shenzhen, China, 2011, pp. 379-383.

[9] B. Li and Max Q.-H. Meng, "Texture analysis for ulcer detection in capsule endoscopy images," *Image Vision Comput*, vol. 27, pp. 1336-1342, 2009.

[10] B. Li and M.Q.-H. Meng, "Analysis of the gastrointestinal status from wireless capsule endoscopy images using local color feature" in *Proc. 2007 Int. Conf. Inf. Acq.*, Jeju City, Korea, 2007, pp. 553–557.

[11] V.S. Kodogiannis, M. Boulougoura, E. Wadge and J.N. Lygouras, "The usage of soft-computing methodologies in interpreting capsule endoscopy," *Eng. Appl. Artif. Intel.*, vol. 20, pp. 539–553, 2007.

[12] Xiaoying Liu, Jia Gu, Yaoqin Xie, Jun Xiong, and Wenjian Qin, "A new approach to detecting ulcer and bleeding in Wireless capsule endoscopy images, " in *Proc. 2012 IEEE-EMBS Int. Conf. Biomed. Health Inform.*, Hong Kong, 2012, pp. 737–740

[13] V.S Charisis *et al.*, "Capsule endoscopy image analysis using texture information from various colour models," *Comput. Methods Programs Biomed.*, vol. 107, no. 1, pp. 61-74, 2012.

[14] V.S. Charisis, L.J. Hadjileontiadis, and G.D. Sergiadis, "Enhanced ulcer recognition from capsule endoscopic images using texture analysis," in *New Advances in the Basic and Clinical Gastroenterology*, T. Brzozowski, Ed. Croatia: InTech, 2012, pp. 185–210.

[15] T. Ojala, M. Pietikainen, and D. Harwood, "A comparative study of texture measures with classification based on feature distributions," *Pattern Recognition,* vol. 29, pp. 51–59, 1996.

[16] T. Ojala, M. Pietikainen, and T. Maenpaa, "Multi-resolution gray-scale and rotation invariant texture classification with local binary pattern," *IEEE Trans. Pattern Analysis and Machine Intelligence*, vol. 24, no. 7, pp. 971–987, 2002.